A&A 531, L11 (2011)
DOI: 10.1051/0004-6361/201116772

Astronomy & Astrophysics

Letter to the Editor

The extent of dust in NGC 891 from *Herschel*/SPIRE images⋆

S. Bianchi[1] and E. M. Xilouris[2]

[1] INAF - Osservatorio Astrofisico di Arcetri, Largo E. Fermi 5, 50125 Florence, Italy
e-mail: sbianchi@arcetri.astro.it
[2] Institute of Astronomy and Astrophysics, National Obs. of Athens, I. Metaxa and Vas. Pavlou, P. Penteli, 15236 Athens, Greece
e-mail: xilouris@astro.noa.gr

Received 23 February 2011 / Accepted 8 June 2011

ABSTRACT

We analyse *Herschel*/SPIRE images of the edge-on spiral galaxy NGC 891 at 250, 350, and 500 μm. Using a 3D radiative transfer model we confirm that the dust has radial fall-off similar to the stellar disk. The dust disk shows a break at about 12 kpc from the centre, where the profile becomes steeper. Beyond this break, emission can be traced up to 90% of the optical disk on the NE side. To the SW, we confirm dust emission associated with the extended, asymmetric HI disk, previously detected by the Infrared Space Observatory (ISO). This emission is marginally consistent with the large diffuse dust disk inferred from radiative transfer fits to optical images. No excess emission is found above the plane beyond that of the thin, unresolved, disk.

Key words. galaxies: individual: NGC 891 – galaxies: spiral – dust, extinction – submillimeter: galaxies – radiative transfer

1. Introduction

The dust distribution in the edge-on galaxy NGC 891 has been studied in detail. Radiative transfer fits to optical/near-infrared (NIR) images have shown that its extinction lane can be described with a dust disk that is radially wider but vertically thinner than the stellar disk. (Because its exponential radial scalelength is 1.5–2 times and the vertical scalelength half that of the stars, so hereafter we call it the *diffuse dust disk*; Xilouris et al. 1998, 1999). This disk is found to have moderate extinction properties, since the central optical depth perpendicular to the disk is about 1 in the B-band. However, this is not large enough to explain the amount of energy emitted by dust and observed in the far-infrared (FIR) and submm spectral energy distribution (SED): the *energy balance* requires that up to three times more starlight is absorbed by dust than predicted by the *diffuse dust disk* (Popescu et al. 2000). Similar dust disk properties and the same *energy balance* problem have been found in other edge-on galaxies (Xilouris et al. 1999; Misiriotis et al. 2001; Dasyra et al. 2005; Bianchi 2007, 2008; Baes et al. 2010).

Radiative transfer models of dust emission in NGC 891 solve the *energy balance* problem by including a second dust distribution associated with the molecular gas, of mass comparable to that of the *diffuse dust disk*. This second component escapes detection in optical images because it is thinner than *diffuse dust* (Popescu et al. 2000, 2011) or it is clumpy in nature, thus producing effects that are less coherent than the extinction lane caused by *diffuse dust* (Bianchi 2008). Hereafter, we call this second component the *clumpy dust disk*. A model for NGC 891 was presented in Bianchi (2008), made with the radiative transfer code TRADING. Though the model includes several features, we found that emission beyond 100 μm is caused mainly by an exponential disk of evolved stars (radial scalelength 4 kpc and vertical scalelength 0.4 kpc, as derived in the NIR by Xilouris et al. 1999) heating at thermal equilibrium both the *diffuse dust disk* (radial scalelength 8 kpc and vertical scalelength 0.2 kpc) and the external envelope of the clouds in the *clumpy dust disk* (with clouds distributed exponentially with the radial scalelength of the stars, and the vertical scalelength of the diffuse dust disk).

In this Letter we compare the structural properties of the dust distribution in NGC 891 inferred indirectly from extinction studies and/or model predictions with those derived from recent submm images taken by the SPIRE instrument (Griffin et al. 2010) aboard the *Herschel* Space Observatory (Pilbratt et al. 2010). In particular, the high sensitivity of SPIRE, together with the edge-on configuration of the galaxy, allow studying submm emission up to large radial distances from the galactic centre. This is needed to directly verify the presence of the diffuse dust disk, whose predicted emission could become visible over that of the clumpy dust disk only in the outskirts of the galaxy.

2. Observations and data reduction

SPIRE photometric observations at 250, 350, and 500 μm were obtained as part of the Guaranteed Time Key Project Very Nearby Galaxy Survey (Wilson). The galaxy was observed in large map mode, covering an area of $20' \times 20'$ centred on the object with two crossscans, using a $30''$ s^{-1} scan rate. Data was retrieved from the *Herschel* Science Archive and reduced with the dedicate software HIPE[1] (Ott 2010). As the current pipeline simply removes median baselines from the timelines, causing artifacts in the maps from the presence of bright extended sources, we subtracted from each bolometer timeline a

⋆ *Herschel* is an ESA space observatory with science instruments provided by European-led Principal Investigator consortia and with important participation from NASA.

[1] We used HIPE 5.2 and the SPIRE calibration tree v. 5.1. SPIRE characteristics (point spread function – PSF – *FWHM* width and beam area, empirical PSF's, calibration uncertainty, and colour corrections) are taken from the SPIRE Observers' Manual (v2.3, 2011).

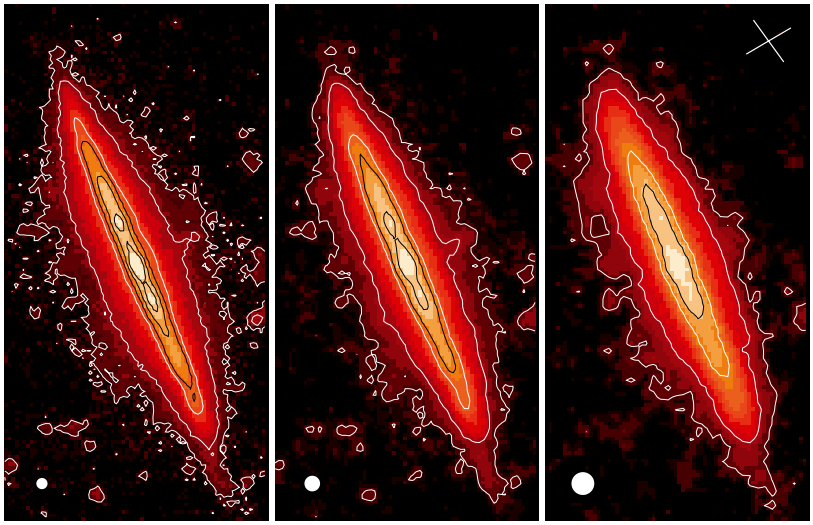

Fig. 1. SPIRE images of NGC 891 at 250 (*left*), 350 (*centre*), 500 μm (*right*). Each panel shows an area of $14' \times 28'$ centred on the galaxy's radio continuum coordinates $\alpha = 2^h22^m33\overset{s}{.}0$, $\delta = 42°20'57\overset{''}{.}2$ (J2000.0; Oosterloo et al. 2007). The main beam size is indicated by the filled circle (*FWHM*: $18\overset{''}{.}1$, $24\overset{''}{.}9$, and $36\overset{''}{.}4$). Images have pixel sizes of 6, 8, 12″ at 250, 350, and 500 μm, respectively (i.e. about 1/3 of the measured *FWHM*). The crossed lines in the 500 μm image show the scan directions. The sky rms noise is $\sigma = 0.74$, 0.44, and 0.23 MJy sr^{-1}, from 250 to 500 μm. Contours are shown at 3, 10, 100, 200-σ over all images, at 500-σ in the 250 and 350 μm map, at 1000-σ only in the 250 μm map. North is up, east to the left.

linear fit obtained *after* carefully masking the data over the region covered by the galaxy. Maps were then produced using the naïve mapmaking procedure within HIPE. The resulting images (Fig. 1) have uniform backgrounds. We also experimented with median baseline removal and the alternative mapmaking software Scanamorphos v7 (Roussel 2011), but found no significant difference for any of the analyses presented here.

3. The data vs. the model

Total flux densities are 169 ± 25, 72 ± 11, and 26 ± 4 Jy, at 250, 350, and 500 μm, respectively. These values include a colour correction appropriate to the observed spectral index ($F_\nu \propto \nu^{2.7}$): since the source is only resolved along the major axis (see later), we used a correction halfway between that for point and extended sources. (We multiplied the pipeline flux densities by 0.94, 0.95, 0.94.) We adopted a very conservative 15% calibration uncertainty for extended emission (see the Observers' Manual, Sect. 5.2.13). Other sources of uncertainty (photometry, point source/extended calibration) are much smaller, $\lesssim$4%.

SPIRE flux densities are shown in Fig. 2, together with the FIR data at 60 and 100 μm from the IRAS satellite and at 170 and 200 μm from the ISO satellite (see Popescu et al. 2011, and references therein), as well as the submm flux densities at 350, 550, and 850 μm from the HFI instrument aboard the *Planck* satellite[2].

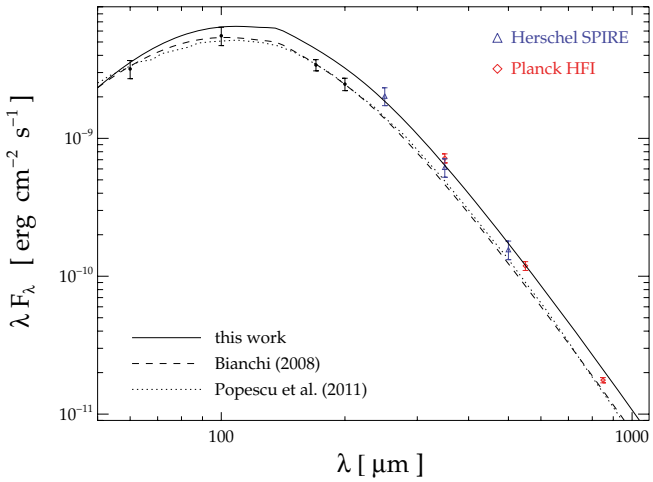

Fig. 2. The integrated FIR-submm SED of NGC 891.

Major axis profiles are shown in Fig. 3. To increase the signal-to-noise ratio, they were averaged over two beams across the plane. Residual sky gradients were estimated from two parallel strips on both sides of the galactic plane, well beyond the emission perpendicular to the major axis. They were found to be smaller than 0.5-σ in all bands, so they do not affect the profiles significantly. Profiles were extracted using a position angle of 22.9°, which was determined with the fitting procedure of Bianchi (2007). The inner profile of the galaxy can be roughly described as the edge-on projection of an exponential disk, with radial scalelength increasing from 4.6 kpc at 250 μm, to 5.1 kpc at 350 μm, and to 5.2 kpc at 500 μm. (We assumed a distance $D = 9.5$ Mpc; van der Kruit & Searle 1981.) A break occurs in all bands at about 12 kpc from the centre ($4\overset{'}{.}4$), after which the profiles become steeper (with a radial scalelength of about 1 kpc). Such radial breaks are analogous to what is found in most stellar disks (Pohlen & Trujillo 2006) and have already been observed with SPIRE (Pohlen et al. 2010). Though the change in slope in NGC 891 is quoted as appearing at about 6′ (coming to a sharp truncation at $7\overset{'}{.}5$; van der Kruit & Searle 1981), the optical images used in Xilouris et al. (1999) indicate a break similar to the one detected for dust. SPIRE clearly improves over previous submm observations. SCUBA was able to detect the dust emission at 850 μm within the radial break only (Alton et al. 1998). The 850 μm morphology for the inner region is very similar to

[2] Since NGC 891 is marginally resolved by *Planck*, we used the flux densities determined by fitting the data with a 2-D Gaussian model, as reported in the Early Release Compact Source Catalogue (Planck Collaboration et al. 2011). The quoted calibration uncertainties are 7% at 350 and 550 μm and 2% at 850 μm (Planck HFI Core Team et al. 2011). Colour corrections for a $\nu^{2.7}$ spectrum were taken from the Catalogue Explanatory Supplement. We did not correct the flux density at 850 μm for the contamination due to the CO(3–2) line. This was found to be about 5% in SCUBA observations (Israel et al. 1999), and it is likely to be lower for the wider 353GHz bandpass. The *Planck* flux density at 350 μm appears to be higher than SPIRE, though still within 1-σ, for the large SPIRE calibration uncertainty adopted here. We do not use other submm observations from the literature (for references, see: Popescu et al. 2011; Bianchi 2008), because they could have been maimed by a limited spatial coverage and uncertain PSF sidelobe corrections. We note, however, that the *Planck* flux density at 850 μm is within the errors of SCUBA observations (Alton et al. 1998; Israel et al. 1999).

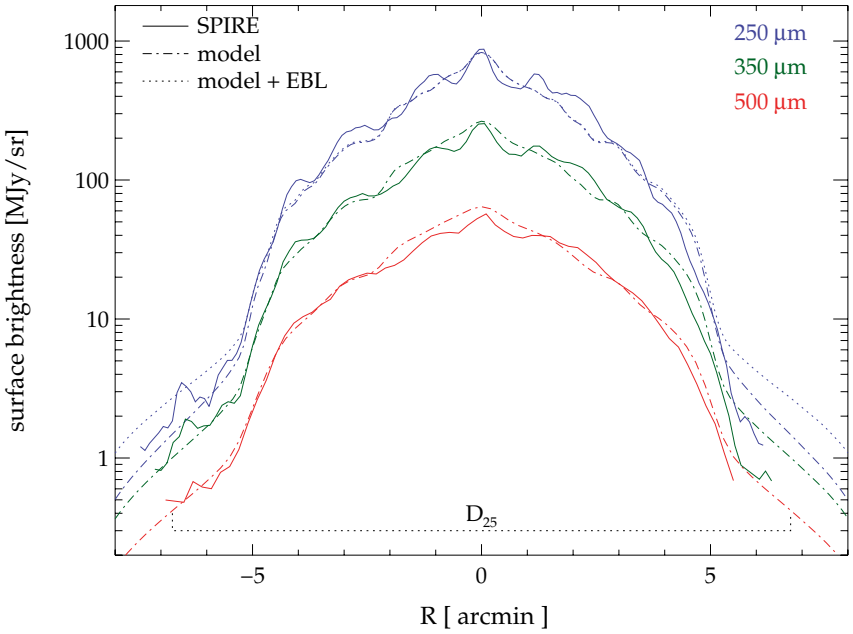

Fig. 3. Surface brightness profiles along the major axis from SPIRE images (solid lines) and the corresponding models by Bianchi (2008) (dot-dashed lines) at 250 (*top*, blue, lines), 350 (*middle*, green, lines), and 500 μm (*bottom*, red, lines). We also show the profile for the model that includes dust heating from the EBL (dotted line, for 250 μm only). For each band, profiles are averaged over two beams perpendicular to the major axis. They are shown for flux densities ≥1.2, 0.75, and 0.45 MJy sr^{-1} for 250, 350, and 500 μm, respectively, corresponding to $S/N > 3$ for the average. Negative distances from the centre refer to the SW end of the galaxy. The optical size of the galaxy (D_{25} = 13.′5; de Vaucouleurs et al. 1991) is indicated. See text for other details.

SPIRE images, and a radial scalelength of 5.3 kpc was fitted to the profile (Alton et al. 2000), close to what we find at 500 μm.

After the break, the profile on the NE side of the galaxy can only be traced up to 6′, or 90% of the optical size (assuming D_{25} = 13.′5 = 37 kpc; de Vaucouleurs et al. 1991). On the SW end, instead, significant emission is seen in excess of the break, up to the optical size and beyond. The excess has already been detected in ISOPHOT images at 170 and 200 μm (Popescu & Tuffs 2003); it corresponds to the SW extension of the asymmetric HI disk, as can be seen by comparing the 3-σ SW appendage of Fig. 1 with the 10^{21} cm^{-2} HI column density contour at a comparable resolution in Fig. 1 of Oosterloo et al. (2007). From the data, we derived a dust mass for this feature of 6×10^5 $M_\odot$ (though with an uncertainty of almost a factor two, mainly because of the difficulty deriving temperatures using only SPIRE fluxes). The HI mass corresponding to the SPIRE detection (estimated from the column density levels in Oosterloo et al. 2007) is about 10^8 $M_\odot$, resulting in a dust-to-gas mass ratio of 0.006, similar to what is found for the inner disks of other galaxies and of the Milky Way (see, e.g., Draine et al. 2007). This confirms that the gas is not pristine, and it supports the view that the lopsidedness of NGC 891 originated from the perturbation of the galactic disk during a fly-by of the nearby companion UGC 1807 (Mapelli et al. 2008). The HI mass for the whole SW disk extension is 2.5×10^8 $M_\odot$. Assuming the same dust-to-gas mass ratio, we estimated a total dust mass of 1.5×10^6 $M_\odot$ for the region. (A similar result was found by Popescu & Tuffs 2003.)

Previous radiative transfer models of NGC 891 underpredict the new submm SED. For instance, the 250 μm flux density predicted by Bianchi (2008) is about 45% lower than observed (see Fig. 2, where we also show the similar, but independent, model of Popescu et al. 2011). We revised the model to describe the submm SED and the radial profiles observed by SPIRE better. Following the procedure of Bianchi (2008), we increased the mass in the *clumpy dust disk* (from 0.5 to 1.1×10^8 $M_\odot$, making up 70% of the total dust mass) and fine-tuned the other parameters (mainly, we raised the galaxy intrinsic luminosity from 7.8 to 8.5×10^8 $L_\odot$) to reproduce the stellar SED as well. The SED of the new model is shown in Fig. 2. It is only marginally consistent with the 100 μm IRAS flux density, and it does not reproduce the 170 and 200 μm flux densities from ISO. With the FIR/submm emissivity of the adopted dust grain model (Draine & Li 2007), and for the interstellar radiation fields implied by the relative geometries of dust and stars assumed within the radiative transfer code TRADING, it was not possible to find a model able to describe all datapoints.

Modelled major axis profiles (Fig. 3) were obtained by convolving simulated images in the three bands with the respective empirical PSFs, regridding them on the chosen pixel size and averaging the profile as for real data. For a match of the broad surface brightness distribution along the major axis (as well as of the SED), we had to use the same radial scalelength (5.7 kpc) both for the *clumpy dust disk* and for the stellar disk. The second result is puzzling, since most of the observed stellar emission (and a good fraction of the absorbed energy in the current model) comes from the NIR, for which the radiative transfer fits found a smaller stellar radial scalelength (4 kpc; Xilouris et al. 1999). Also, as already noted in Bianchi (2008), emission from the clumpy dust disk appears smoother than the real data, revealing that dust inhomogeneities on a larger scale than molecular clouds (i.e. rings, spiral arms) should be considered in models.

The break in the profile is reproduced in the model by a sharp cut of both the clumpy dust disk and the stellar disk at 13 kpc from the centre (4.7′ in Fig. 3)[3]. Beyond the break, the modelled emission is only due to the diffuse dust disk derived from optical observations. The mean dust temperature in this disk is low ($10 < T < 13$ K) because the heating sources (mainly stars at the edge of the disk; the bulge contribution is negligible) are no longer mixed with dust. The predicted surface brightness matches the observations only on the SW, where emission comes from the excess previously described. The axisymmetric diffuse dust disk derived by Xilouris et al. (1999) could thus mimic the contribution to extinction of the (asymmetric) extended HI component. However, it is to be noted that the model predicts a lower temperature than what is derived in the SW appendage (15 K), and the mass of the *diffuse dust disk* beyond 13 kpc (8×10^6 $M_\odot$) is 5× higher than what is estimated from the HI data, which is too high a factor to be explained by the uncertainties in the temperature and in the various model assumptions. Also, model

[3] Conversely, the break could be produced by truncating the *clumpy dust disk* only, if the model did not include a *diffuse dust disk*.

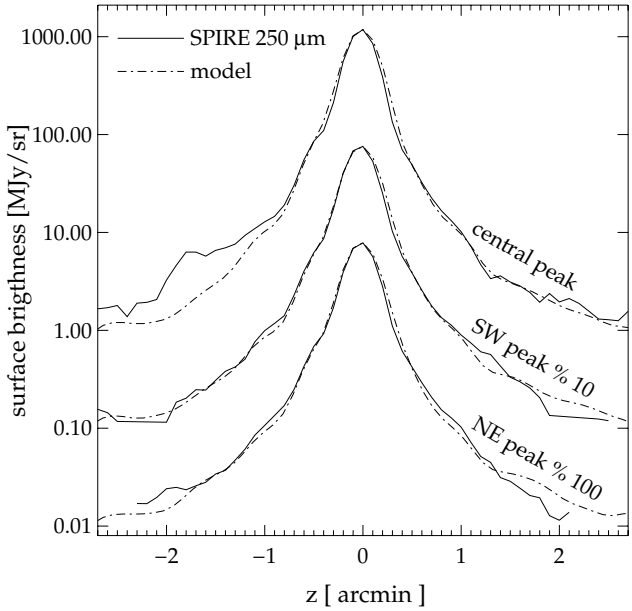

Fig. 4. Data and (scaled) model profiles at 250 μm perpendicular to the major axis through the centre of the galaxy and the two secondary peaks. The profile through the SW peak has been divided by 10, that in the NE by 100). Negative heights refer to the NW side of the disk.

predictions are likely lower limits to the real emission from a diffuse dust disk. If stars extend more than what is needed to fit the radial break, the emission will be higher. Instead, if grains are isolated from stars, the extragalactic background light (EBL) might contribute significantly. The dotted line in Fig. 3 shows the effect on the 250 μm profile of the EBL P1.0 model of Aharonian et al. (2006). Emission from the diffuse dust disk in this region of the model could rise by a factor two[4].

Finally, Fig. 4 shows the 250 μm profiles perpendicular to the major axis, for three cuts passing through the galaxy centre and the two secondary peaks at about 1′ from the centre on the NE and SW. Data were averaged over two beams perpendicular to the cut, and a residual background was subtracted from regions beyond the emission. Model profiles were scaled to match the data on the major axis. Emission above the plane is almost entirely dominated by the PSF Airy rings picking up light from the major axis (because the adopted dust vertical scalelength, 0.2 kpc or 4″, is much smaller than the main beam). Results are similar in the other SPIRE bands. Excess emission is only seen on the NW side of the minor axis profile, in coincidence with the background X-ray source CXO J022224.4+422138, which contributes to most of the excess; however, part of it could come from another background source aligned with the minor axis or from a filamentary structure protruding from the galactic centre. Excluding this feature, SPIRE images do not show evidence of any diffuse halo emission. This is at odds with the previous Spitzer observations of Burgdorf et al. (2007), which detected MIR emission extending up to 5 kpc from the plane. At 22 μm, a surface brightness of 0.1–0.2 MJy/sr is found at 1–1.′4 along the minor axis. Instead, at 250 μm, residual emission from the halo is less than 1 MJy/sr. Such MIR/submm flux density ratios can be produced by typical Milky Way dust, if the interstellar radiation field is 10× higher than the local (see, e.g., Fig. 13 in Draine & Li 2007). These heating conditions might be compatible with the hypothesis that the detected MIR radiation come from dust surrounding halo AGB stars (Burgdorf et al. 2007).

[4] The temperature of dust heated by the EBL only is about 11 K, adopting mean dust properties from Draine & Li (2007).

4. Summary and conclusions

We have analysed SPIRE observations of the edge-on spiral galaxy NGC 891 and examined both their contribution to the galaxy's SED and the galaxy's morphological properties at these wavelengths. Emission within the central 4.′4 broadly follows a radial exponential distribution with a scalelength similar to those derived for the stars in the surface brightness fits of Xilouris et al. (1999). Emission above the galactic plane can be explained with radiation from the galactic plane picked up by the PSF wings. The distribution of dust along the vertical direction is thus thinner than the SPIRE PSFs, and compatible with the vertical scalelength derived by Xilouris et al. (1999).

Beyond 4.′4 from the centre, the radial profile shows a break and becomes steeper. On the NE side, the submm disk comes to an end within the optical size of the galaxy. Instead, on the SW side the profile decline is interrupted at about the optical radius, where significant emission is seen in all bands. With their high resolution, SPIRE observations confirm the excess emission associated with the asymmetric HI disk, already found in deep ISOPHOT observations by Popescu & Tuffs (2003).

The emission within the central 5′ can be attributed to the *clumpy dust disk* required by radiative transfer models to fit the FIR/submm SED of the galaxy (Bianchi 2008). The HI-associated dust emission in the SW instead has surface brightness levels that are marginally consistent with those predicted for the *diffuse dust disk*, an important dust component (of similar mass to that of the clumpy dust disk) responsible for the optical/NIR extinction lane (Xilouris et al. 1999). Since extended *diffuse dust disks* are routinely found in optical/NIR radiative transfer fits of edge-on galaxies, we hope that further *Herschel* observations of these objects (as those planned within the approved projects HEROES and NHEMESES), together with radiative transfer models and deep observations of their atomic gas disks, will help for understanding if the diffuse dust disk is indeed a component associated with the atomic gas and is a feature common to all spiral galaxies.

References

Aharonian, F., Akhperjanian, A., Bazer-Bachi, A., et al. 2006, Nature, 440, 1018
Alton, P. B., Bianchi, S., Rand, R. J., et al. 1998, ApJ, 507, L125
Alton, P. B., Xilouris, E. M., Bianchi, S., et al. 2000, A&A, 356, 795
Baes, M., Fritz, J., Gadotti, D. A., et al. 2010, A&A, 518, L39
Bianchi, S. 2007, A&A, 471, 765
Bianchi, S. 2008, A&A, 490, 461
Burgdorf, M., Ashby, M. L. N., & Williams, R. 2007, ApJ, 668, 918
Dasyra, K., Xilouris, E., Misiriotis, A., & Kylafis, N. 2005, A&A, 437, 447
de Vaucouleurs, G., et al. 1991, Third Reference Catalogue of Bright Galaxies (Berlin: Cambridge University Press), RC3
Draine, B. T., & Li, A. 2007, ApJ, 657, 810
Draine, B. T., Dale, D. A., Bendo, G., et al. 2007, ApJ, 663, 866
Griffin, M. J., Abergel, A., Abreu, A., et al. 2010, A&A, 518, L3
Israel, F. P., van der Werf, P. P., & Tilanus, R. P. J. 1999, A&A, 344, L83
Mapelli, M., Moore, B., Ripamonti, E., et al. 2008, MNRAS, 383, 1223
Misiriotis, A., Popescu, C. C., Tuffs, R., & Kylafis, N. D. 2001, A&A, 372, 775
Oosterloo, T., Fraternali, F., & Sancisi, R. 2007, AJ, 134, 1019
Ott, S. 2010, ASP Conf. Ser., 434, 139
Pilbratt, G. L., Riedinger, J. R., Passvogel, T., et al. 2010, A&A, 518, L1
Planck Collaboration, Ade, P. A. R., Aghanim, N., et al. 2011, A&A, accepted [arXiv:1101.2041]
Planck HFI Core Team, Ade, P. A. R., Aghanim, N., et al. 2011, A&A, submitted [arXiv:1101.2048]
Pohlen, M., & Trujillo, I. 2006, A&A, 454, 759
Pohlen, M., Cortese, L., Smith, M. W. L., et al. 2010, A&A, 518, L72
Popescu, C. C., & Tuffs, R. J. 2003, A&A, 410, L21
Popescu, C. C., Misiriotis, A., Kylafis, N. D., et al. 2000, A&A, 362, 138
Popescu, C. C., Tuffs, R. J., Dopita, M. A., et al. 2011, A&A, 527, A109
Roussel, H. 2011, A&A, submitted
van der Kruit, P. C., & Searle, L. 1981, A&A, 95, 105
Xilouris, E. M., Alton, P. B., Davies, J. I., et al. 1998, A&A, 331, 894
Xilouris, E. M., Byun, Y. I., Kylafis, N. D., et al. 1999, A&A, 344, 868